Finite Element Modeling of Brushless Doubly-Fed Induction Machine Based on Magneto-Static Simulation

Xuezhou Wang, Tim D. Strous, Domenico Lahaye, Henk Polinder, *Senior Member, IEEE,* Jan A. Ferreira, *Fellow, IEEE*

***Abstract*—The brushless doubly-fed induction machine (BDFIM) is a potentially attractive choice for a variable-speed wind generator. Using classical analytical models is not so straightforward, because the motion of the magnetic field in BDFIM is not a simple rotation. Finite element (FE) modeling makes it easier to evaluate the machine performance considering the saturation. However, for the purpose of a better convergence and an accurate calculation of the magnetic field equation and the coupled circuit equation, small time steps are utilized in the adaptive time-step solver of the transient FE model. A long computing time makes FE model be difficult to combine with an optimization program. This paper presents one possible alternative method to predict the BDFIM performance by using the magneto-static FE solutions and the space-time transformation. The simulation time then reduces significantly making it possible to search in a large design space for the optimization purpose.**

***Index Terms*—Brushless, cross-coupling, doubly-fed, finite element modeling (FEM), induction machine, magneto-static simulation, nested-loop rotor, space-time transformation.**

I. Introduction

THE doubly fed induction machine (DFIM) is currently the most common generator for wind turbines. It has the advantage of operating at variable speed with only a fractionally rated power converter. However, its main drawbacks are low grid-fault ride-through ability and low reliability because of the brush and the slip rings [1].

The idea of brushless doubly fed induction machine (BDFIM) came from the self-cascaded machine. The concept of the modern BDFIM is essentially the same as that proposed by Burbridge and Broadway [2]. As the name implies, the BDFIM has two stator AC supplies with different pole-pairs to avoid their direct magnetic coupling. The magnetic coupling is achieved through a special rotor like Fig. 1. Fig. 2 shows a typical structure of BDFIM. One of the stator windings is referred to as the power winding which is connected with the grid directly. The other one is called the control winding which is connected to the grid through a partially rated converter giving a variable frequency and voltage. Generally, the rating of the converter is chosen as about one third of the rating of the machine which allows a speed variation of about $\pm 30\%$ [3].

BDFIM is attractive because it shares with the same advantages of DFIM, but eliminates the need for the brush and the slip rings [4]. In addition, the BDFIM also shows a better fault ride-through capability [5]. Considering its benefits, one likely application for the BDFIM is a new generator in wind turbines, especially for off-shore installations.

However, on the other hand, the BDFIM also has some disadvantages such as higher manufacturing cost, a slightly larger dimension and lower efficiency comparing with DFIM with same rating [6]. Therefore, it is very important to find a better modeling and design for the BDFIM to make it commercially exploitable. Equivalent circuit theory is simple for analysis and optimization of BDFIM [7]. Furthermore, some analytical methods including harmonic analysis [8] or reluctance networks [9] have been proposed to model BDFIM. The air-gap contains two main magnetic fields with different pole-pair numbers and different frequencies resulting in a complex distribution of the magnetic field in this special machine. Therefore, the above analytical models are not so straightforward to take the nonlinearity into account while the machine is normally designed to work in a little bit saturation in order to make sufficient use of the materials.

From the point of accuracy, finite element (FE) modeling has the advantages of considering the complex geometry and the nonlinear effect. Transient FE simulation is applied to the BDFIM in [10]. However, it needs small time steps to solve the electromagnetic diffusion equations and the induced rotor currents. This makes it quite time consuming and difficult to be combined with the optimization progress. Several methods are proposed for a fast FE calculation called as computationally efficient finite-element analysis (CE-FEA) [11] or ultrafast finite-element analysis [12] and have been applied to analyze PM machines.

The aim of this paper is to present one possible alternative way to model BDFIM by using the magneto-static FE simulations. The electromagnetic diffusion equation is reduced to a quasi-Poisson equation by assuming the electrical conductivity to be zero in the computing domains. We derived the space-time relationship of the stator magnetic field and its induced rotor currents analytically. Considering the symmetry of the magnetic circuit and the periodicity of the electromagnetic

The research leading to these results has received funding from the European Union's Seventh Framework Programme managed by REA - Research Executive Agency (FP7/2007_2013) under Grant Agreement N.315485.

The research leading to these results has received funding from the China Scholarship Council for supporting X. Wang's PhD research work.

X. Wang, T. D. Strous, H. Polinder and J. A. Ferreira are with the Department of Electrical Sustainable Energy, Delft University of Technology, Delft, The Netherlands, (email: X.Wang-3@tudelft.nl, T.D.Strous@tudelft.nl, H.Polinder@tudelft.nl, J.A.Ferreira@tudelft.nl).

D. Lahaye is with the Delft Institute of Applied Mathematics, Delft University of Technology, Delft, the Netherlands, (email: D.J.P.Lahaye@tudelft.nl).

978-1-4799-7940-0/15/$31.00 ©2015 IEEE

Fig. 1. Nested-loop rotor structure [4]

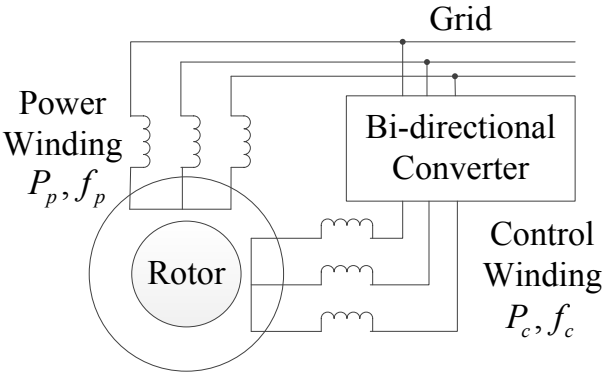

Fig. 2. The structure of BDFIM

field, the rotor currents can be calculated using one separate static simulation which makes it independent on the size of the time step. The number of the magneto-static simulations depends on the highest frequency component considered for the core losses calculation. The results show that the proposed method can predict the BDFIM performance accurately, but it can reduce the simulation time significantly comparing with the expensive transient simulation. Furthermore, from the point of approximation, only one magneto-static simulation is also possible for the performance prediction which can further save the computing time. The model presented in this paper has been applied for the optimization of the prototype [13].

This paper starts with a brief introduction of the BDFIM operating principles, as well as the magnetic field created by the stator windings. The space-time relationship of the magnetic field in the rotor reference is derived. Next, to the FE modeling, the equations of the magneto-static field are derived and the methods to calculate the rotor currents, electromagnetic torque and losses using the magneto-static FE solutions are described. Subsequently, the simulation results are shown comparing with the transient results. Finally, conclusions are drawn.

II. Theoretical Background

A. BDFIM Operating Principles and Specifications

The basic operating principle of BDFIM is illustrated briefly in this section. The key point to this machine is the cross-coupling between the power winding and the control winding through a special rotor. One common rotor structure is the nested-loop configuration.

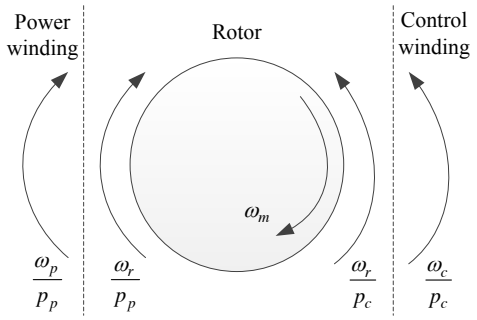

Fig. 3. Rotating speed of stator and rotor fundamental fields in BDFIM

TABLE I
Main Specifications of the Studied BDFIM

Description	Machine parameter	Value
Axial length [m]	l_{stk}	1.596
Air-gap length [mm]	l_g	1.5
Stator outer radius [m]	r_{so}	0.83
Stator inner radius [m]	r_{si}	0.67
Rotor inner radius [m]	r_{ri}	0.58
Number of phases	N_{ph}	3
Number of pole-pairs	p_p, p_c	4, 6
Rated frequency [Hz]	f_p, f_c	50, 10
Number of stator slots	N_{ss}	72
Number of rotor nests	N_{nest}	10
Number of loops per nest	q_r	3
Rotational speed [rad/s]	ω_m	37.7
Rated power [MW]	P	3.0

We assume that the power winding has p_p pole-pairs and frequency ω_p. And the control winding has p_c pole-pairs and frequency ω_c. According to Fig. 3, considering the rotor mechanical angular velocity ω_m, the frequencies of the rotor currents induced by the power winding and control winding are respectively as:

$$\omega_{rp} = \omega_p - p_p\omega_m, \tag{1}$$

$$\omega_{rc} = \omega_c + p_c\omega_m. \tag{2}$$

The cross-coupling actually requires the frequencies of rotor currents induced by the power winding and control winding should be the same:

$$(\omega_p - p_p\omega_m) = \pm(\omega_c + p_c\omega_m). \tag{3}$$

Therefore,

$$\omega_m = \frac{\omega_p - \omega_c}{p_p + p_c} \quad (or \quad \omega_m = \frac{\omega_p + \omega_c}{p_p - p_c}). \tag{4}$$

The first condition is preferred in the wind turbines applications. Because it leads to a lower 'synchronism natural speed' ($\omega_c = 0$). Less stage of gear-box would be needed. In addition, the cross-coupling also requires the number of rotor nests N_{nest} should equal to $(p_p + p_c)$. This will be explained in the following section. For the analysis and simulation, Table I gives the main specifications of the studied BDFIM.

B. The Space-Time Transformation

The magnetic fields created by the stator windings are derived in this section. By being rewritten in the rotor reference frame, this field shows some characteristics like a standing wave and one space-time relationship can be obtained. For the ease of derivation, the magnetic flux density B_g in the air-gap produced by the stator windings can be expressed as follows:

$$B_{gp}(t,\theta_s) = \hat{B}_{gp}\cos(\omega_p t - p_p\theta_s + \varphi_p), \tag{5}$$

$$B_{gc}(t,\theta_s) = \hat{B}_{gc}\cos(\omega_c t + p_c\theta_s + \varphi_c), \tag{6}$$

where θ_s is the angle along the stator circumference and φ_p and φ_c are the initial phase angle of the power winding and the control winding respectively. They can also expressed in a coordinate reference frame fixed to the rotor by using:

$$\theta_s = \theta_r + \omega_m t, \tag{7}$$

where θ_r is the angle along the rotor circumference.

$$B_{gp}(t,\theta_r) = \hat{B}_{gp}\cos((\omega_p - p_p\omega_m)t - p_p\theta_r + \varphi_p), \tag{8}$$

$$B_{gc}(t,\theta_r) = \hat{B}_{gc}\cos((\omega_c + p_c\omega_m)t + p_c\theta_r + \varphi_c), \tag{9}$$

The frequency of the electric quantities in the rotor can be defined by:

$$\omega_r = \omega_p - p_p\omega_m = \frac{p_c\omega_p + p_p\omega_c}{p_p + p_c}. \tag{10}$$

Then the flux density created by stator winding in rotor reference frame ((8), (9)) can be rewritten as:

$$B_{gp}(t,\theta_r) = \hat{B}_{gp}\cos(\omega_r t - p_p\theta_r + \varphi_p), \tag{11}$$

$$B_{gc}(t,\theta_r) = \hat{B}_{gc}\cos(\omega_r t + p_c\theta_r + \varphi_c). \tag{12}$$

For the ease of computation, we assumed that $\hat{B}_{gp} = \hat{B}_{gc} = \hat{B}_g$. The total flux density B_{gs} due to these two stator windings can be written as:

$$\begin{aligned} B_{gs}(t,\theta_r) = 2\hat{B}_g\cos(-\frac{p_p + p_c}{2}\theta_r + \frac{\varphi_p - \varphi_c}{2}) \\ \cdot\cos(\omega_r t - \frac{p_p - p_c}{2}\theta_r + \frac{\varphi_p + \varphi_c}{2}). \end{aligned} \tag{13}$$

[14] (Fig. 2) shows a example of such a flux density. He indicates that, in the rotor reference frame, the flux density created by stator windings has some characteristics of a standing wave which has frequency ω_r and $(p_p + p_c)$ poles. It is optimally coupled by a rotor which has the same number of poles. Therefore, for a commonly used nested-loop rotor structure, the number of nests N_{nest} equals to $(p_p + p_c)$. Furthermore,

$$\begin{aligned} B_{gs}(t,\theta_r - 2\tau) = 2\hat{B}_g\cos(-\frac{p_p + p_c}{2}(\theta_r - 2\tau) + \frac{\varphi_p - \varphi_c}{2}) \\ \cdot\cos(\omega_r t - \frac{p_p - p_c}{2}(\theta_r - 2\tau) + \frac{\varphi_p + \varphi_c}{2}), \end{aligned} \tag{14}$$

where

$$\tau = \frac{2\pi}{p_p + p_c}. \tag{15}$$

Therefore,

$$\begin{aligned} B_{gs}(t,\theta_r - 2\tau) = 2\hat{B}_g\cos(-\frac{p_p + p_c}{2}\theta_r + \frac{\varphi_p - \varphi_c}{2}) \\ \cdot\cos(\omega_r t - \frac{p_p - p_c}{2}\theta_r + (p_p - p_c)\tau + \frac{\varphi_p + \varphi_c}{2}), \end{aligned} \tag{16}$$

$$\begin{aligned} B_{gs}(t + \frac{p_p - p_c}{\omega_r}\tau,\theta_r) = 2\hat{B}_g\cos(-\frac{p_p + p_c}{2}\theta_r + \frac{\varphi_p - \varphi_c}{2}) \\ \cdot\cos(\omega_r t + (p_p - p_c)\tau - \frac{p_p - p_c}{2}\theta_r + \frac{\varphi_p + \varphi_c}{2}). \end{aligned} \tag{17}$$

We can see:

$$B_{gs}(t,\theta_r - 2\tau) = B_{gs}(t + \frac{p_p - p_c}{\omega_r}\tau,\theta_r). \tag{18}$$

Then the induced rotor current due to B_{gs} will also support the similar relationship:

$$I_r(t,\theta_r - 2\tau) = I_r(t + \frac{p_p - p_c}{\omega_r}\tau,\theta_r) \tag{19}$$

Equation (18) and (19) mean, in the rotor reference frame, the flux density and its induced rotor current at the position $(\theta_r - 2\tau)$ which is 2τ behind the position θ and the instant t time equals to that at the position θ_r and the instant $(t + \frac{p_p - p_c}{\omega_r}\tau)$ time which is $\frac{p_p - p_c}{\omega_r}\tau$ time before t moment. This relationship gives the ideas of the rotor current calculation and an approximate way for the rotor core losses calculation in the FE modeling section.

III. Finite Element Modeling

A. Assumptions

We have two assumptions throughout the modeling for the purpose of simplification. The first one is that the field due to the eddy-current in the stator and rotor core has little influence on the main field. These eddy-currents are ignored during the calculation while the core losses are computed in the post-processing. This is guaranteed because the eddy-currents are reduced significantly due to the lamination structure in the core. The second one is that the skin-effect and the proximity-effect are ignored for the stator windings and solid rotor bars. This will be investigated separately in the later paper. These two assumptions lead to the electric conductivity as zero in the computing domains. They are also useful to avoid too dense mesh since we pursue saving time.

B. Transient FE Model

The main magnetic field are created by the stator and rotor currents flowing in the axial direction. In this case, we may put our problem on a domain in the xy-plane which could be the cross-section perpendicular to the axial direction and all field quantities are assumed to be z-independent. The two-dimensional electromagnetic field equation is:

$$\frac{\partial}{\partial x}(\frac{1}{\mu}\frac{\partial A_z}{\partial x}) + \frac{\partial}{\partial y}(\frac{1}{\mu}\frac{\partial A_z}{\partial y}) = J_{e,z}. \tag{20}$$

where μ is the permeability of the material, A_z is the z component of the magnetic vector potential and J_e, z is the externally applied current density. The electric conductivity σ is set as zero as mentioned before. The rotor rotation is modeled by using Arbitrary Lagrangian-Eulerian (ALE) formulation in the transient model.

The rotor currents can be calculated by regarding the stator currents as the source currents while the rotor currents are regarded as the induced currents. Then the following external

circuit equation could be coupled with (20) to relate the unknown rotor currents with the resultant magnetic field.

$$\frac{l_{stk}}{S_{bar}}\frac{d(\iint A_z dS_+ - \iint A_z dS_-)}{dt} - I_r R_{bar} = 0, \quad (21)$$

where l_{stk} is the machine axial length, S_{bar} is the cross-sectional area of the rotor bar, I_r is the instant rotor currents, R_{bar} is the resistance of one rotor bar, S_+ and S_- are the surface of the go and return conductors respectively. The time-step is adaptive depending on the accuracy you want and the convergence in most commercial software. We may increase the time-step for a fast simulation but at the expense of accuracy. It is more worse that the convergence sometimes crashes.

C. Magneto-Static FE Model

The static electromagnetic field equation is the same as (20). The instantaneous rotor position can be achieved by rotating the geometry manually corresponding to the instantaneous time moment in the previous transient model. An alternative way can be used for the rotor current calculation to make it independent on the size of time-step. We may consider the main component of rotor currents with fundamental frequency ω_r as an example:

$$\frac{l_{stk}}{S_{bar}}(\iint A_z dS_+ - \iint A_z dS_-)\cdot\omega_r - I_{rs}R_{bar} = 0. \quad (22)$$

where I_{rs} has the same amplitude and frequency with I_r, but with 90 degree phase shift. Suppose we get the instantaneous current at t_1 moment and θ_{r1} position from (22). If we formulate it as:

$$I_{rs}(t_1, \theta_{r1}) = \hat{I}_{rs}\sin(\omega_r t_1 + \varphi_0), \quad (23)$$

We can also get an instantaneous current at t_1 moment but another position $\theta_{r1} - 2\tau$ from the same static result. According to the space-time transformation (19), we have:

$$\begin{aligned} I_{rs}(t_1, \theta_{r1} - 2\tau) &= I_{rs}(t_1 + \frac{p_p - p_c}{\omega_r}\tau, \theta_{r1}) \\ &= \hat{I}_{rs}\sin(\omega_r(t_1 + \frac{p_p - p_c}{\omega_r}\tau) + \varphi_0). \end{aligned} \quad (24)$$

Two unknowns $\hat{I}_{rs}$ and φ_0 can be solved by (23) and (24). Then the applied rotor current I_r at t_1 moment and θ_{r1} position can be expressed as:

$$I_r(t_1, \theta_{r1}) = \hat{I}_{rs}\cos(\omega_r t_1 + \varphi_0). \quad (25)$$

D. Electromagnetic Torque and Power

Maxwell's stress tensor method indicated by (26) and virtual work method are mainly used for the toque calculation.

$$T_e = \frac{l_{stk}}{\mu_0}\int_0^{2\pi} r^2 B_r B_t d\theta, \quad (26)$$

where μ_0 is the permeability of the vacuum, r is the radius of the air-gap, B_r and B_t are the radial and tangential components of the flux density in the air-gap. We only calculate the main torque due to p_p and p_c pole-pair fields as the average torque. The torque ripple is not considered in our study. The flux density can be analytically expressed in Fourier series:

$$B_r(\theta) = B_{r0} + \sum_{n=1}^{\infty}[a_{rn}\cos(n\theta) + b_{rn}\sin(n\theta)] \quad (27)$$

$$B_t(\theta) = B_{t0} + \sum_{n=1}^{\infty}[a_{tn}\cos(n\theta) + b_{tn}\sin(n\theta)] \quad (28)$$

The torque due to n^{th} component can be calculated as:

$$T_n = \frac{\pi r^2 l_{stk}}{\mu_0}(a_{rn}a_{tn} + b_{rn}b_{tn}) \quad (29)$$

Then the main torque can be calculated as:

$$T_{main} = T_{p_p} + T_{p_c} \quad (30)$$

Finally, the calculation of the main electromagnetic power is straightforward:

$$P_{main} = T_{main}\cdot\omega_m. \quad (31)$$

E. Losses and Efficiency Calculation

As analyzed before, there exist two rotating field due to the power winding and the control winding without direct magnetic coupling in the stator. The stator magnetic field has two fundamental frequencies (i.e. f_p, f_c). General speaking, f_c is smaller than f_p which means the time oscillation of the p_p pole-pair component is superimposed on that of p_c pole-pair component. Therefore, the eddy-current losses include two components due to p_p and p_c pole-pair fields. The hysteresis loss is considered by approximately assuming the magnetic field in the stator core as a pure sinusoidal waveform with the amplitude B_{eq} and the frequency f_p [15]. The stator core losses can be evaluated by Modified Steinmetz Equation (MSE) as:

$$P^s_{core} = k_e(f_p^2 B^2_{p,max} + f_c^2 B^2_{c,max})v_s + k_h f_p^{\alpha} B_{eq}^{\beta} v_s, \quad (32)$$

where,

$$B_{eq} = \sqrt{B^2_{p,max} + B^2_{c,max}}, \quad (33)$$

v_s is the volume of the stator core in unit of m^3, α and β are material-dependent constant exponents, k_e and k_h are the eddy current loss factor and the hysteresis loss factor, respectively. They two are in unit of which to make the P^s_{core} in unit of W.

In the rotor reference frame, the variation of the magnetic field has some characteristics of a standing wave. The variations of the flux density of different parts in the rotor yoke and teeth have the same fundamental frequency (i.e. f_r), but with different amplitudes. Note that, according to (18), the distribution and variation of the flux density in each nest are approximate same but with some time delay. If we only consider the fundamental component, the rotor core losses can be calculated as:

$$P^r_{core} = k_e f_r^2 B^2_{rotor,max} v_r + k_h f_r^{\alpha} B^{\beta}_{rotor,max} v_r, \quad (34)$$

where v_r is the volume of the rotor core in unit of m^3. All the specifications of electric steel used in stator and rotor

TABLE II
SPECIFICATIONS OF LAMINATED CORE(M800-65A) [15]

Description	Parameter	Value
Hysteresis loss factor	k_h	273.2
Eddy current loss factor	k_e	0.4786
Lamination thickness [mm]	d_t	0.65
Resistivity [nΩm]	ρ	390
MSE constant	α	1.2558
MSE constant	β	1.685

core are given in Table II. The copper losses calculation is straightforward as:

$$P_{copper}^{s(r)} = I_{s(r)}^2 R_{s(r)} \tag{35}$$

Then the efficiency is calculated as:

$$\eta = \frac{P_{main}}{P_{main} + P_{core}^{s} + P_{core}^{r} + P_{copper}^{s} + P_{copper}^{r}} \tag{36}$$

F. Choice of the Number of Magneto-Static Simulation

The main principle of choosing the number of the magneto-static simulation is based on the sampling theorem. It states that the waveform information would not be lost in the sampling process if it is sampled at least twice the frequency of its highest harmonic. $1/f_c$ is simulated to cover all three frequency components (f_c=10 Hz, f_r=26 Hz, f_p=50 Hz). If we calculate n points during $1/f_r$, the total minimal points during $1/f_c$ are $(f_r/f_c)n$ which determined by:

$$(f_r/f_c)n > 2(f_p/f_c), \tag{37}$$

where $(f_r/f_c)n$ should be an integer. Therefore, in this case study, the minimal 13 magneto-static simulations with same time interval are enough for an approximate prediction of the core losses. Wherein, any consecutive five simulation results are used for the time FFT of f_r component and the total thirteen results are for the time FFT of f_p and f_c components.

However, from the point of approximation, only one magneto-static simulation is possible to estimate the performance. To the rotor side, one static simulation can give $(p_p + p_c)/2$ points along the rotor circumference with same space interval 2τ. According to the space-time relationship indicated by equation(18), these $(p_p + p_c)/2$ points are with same time interval $\tau(p_p - p_c)/\omega_r$ in one rotor electrical cycle $1/f_r$. It means one magneto-static simulation is enough to approximately estimate the rotor core losses if we only take its fundamental frequency component into account. To the stator side, the amplitude of the flux densities for p_p and p_c pole-pair fields can be obtained by doing space FFT to the flux densities of all teeth and their corresponding yoke parts. Then the stator core losses can be calculated by (32).

IV. RESULTS AND DISCUSSION

A. Comparison of Calculated Rotor Currents

Fig. 4 shows the rotor currents obtained from the transient results and the magneto-static results. The rotor is rotated

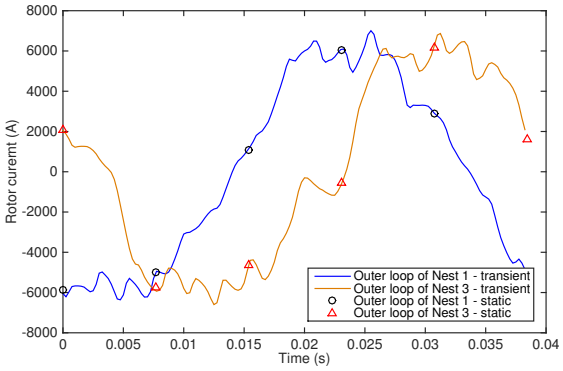

(a) Currents in the outer loop of nest 1 & 3

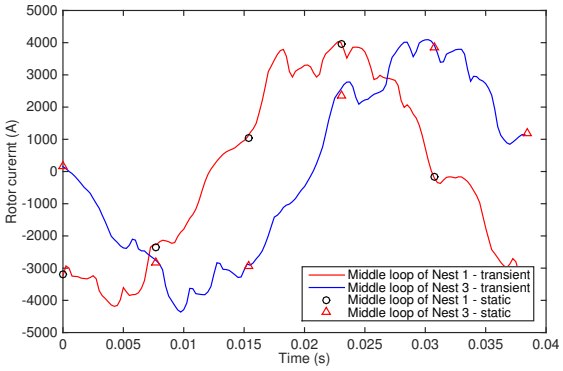

(b) Currents in the middle loop of nest 1 & 3

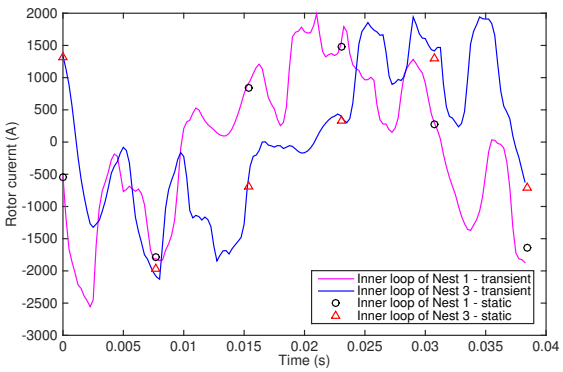

(c) Currents in the innet loop of nest 1 & 3

Fig. 4. Rotor currents calculated in transient and magneto-static simulations

manually in the static simulation with respect to the time in the transient model. Obviously, each instant value of the static result is very close to the transient case. We can obtain the information for further calculation by doing FFT to these discrete points. The number of the discrete points depends on the highest frequency we would like to recover. The currents in the first nest and the third nest have some phase shift which theoretically expressed by (19) if the fundamental component is considered. Fig. 5 gives the time FFT results of the rotor currents corresponding to those in Fig. 4 which calculated by the transient model. Fig. 5 (a) and (b) again prove that the currents flowing in the first and third nests are with similar amplitude, as well as the time-harmonic orders. Moreover, the

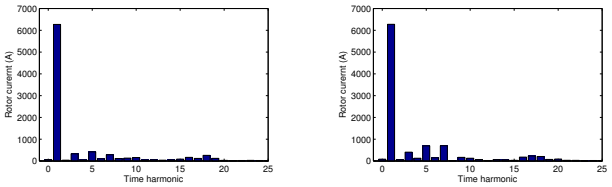

(a) Outer loop of nest 1 (b) Outer loop of nest 3

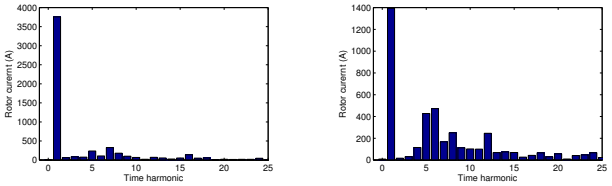

(c) Middle loop of nest 1 (d) Inner loop of nest 1

Fig. 5. Time FFT of rotor currents

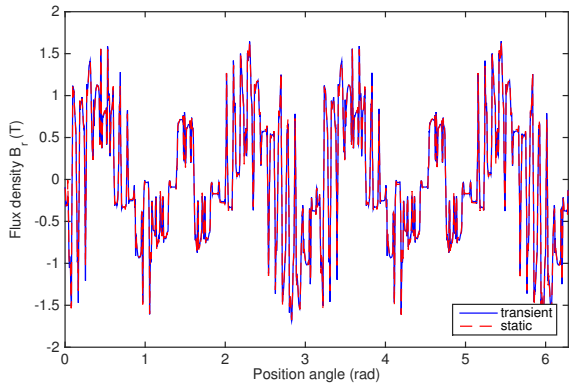

Fig. 6. Total air-gap flux density in the radial direction

current with the fundamental frequency f_r dominates in each loop which ensures our magneto-static model be valid for the calculation. We can also find the outer loop flows much higher current than the inner one which means the outer loop makes more contribution to the torque.

B. Comparison of Air-gap Magnetic Field

Fig. 6 gives the comparison of the total flux density in the radial direction between the transient simulation and the proposed alternative way at one time point. It is not difficult to understand the good agreement between them since the applied stator currents are the same and the calculated rotor currents are so close to each other (show in Fig. 4). However, some little divergence are still there because the calculated rotor currents are not exactly the same in these two models.

C. Performance Comparison

The BDFIM performances estimated by the transient simulations and the magneto-static simulations are listed in Table III. The proposed FE model based on the magneto-static simulation provides the predictions at the same accurate level like the transient simulation. But it reduces the computing time dramatically which makes it possible to be combined with the

TABLE III
BDFIM PERFORMANCE PREDICTION - $q_r = 3$

Performance	Transient	13 static	error	1 static	error
Torque [kN·m]	85.202	84.229	1.1%	84.791	0.5%
Power [MW]	3.2121	3.1754	1.1%	3.1966	0.5%
Stator core losses [kW]	68.955	64.706	6.2%	65.475	5.0%
Rotor core losses [kW]	18.541	16.962	8.5%	16.282	12.2%
Stator copper losses [kW]	79.561	79.561	-	79.561	-
Rootr copper losses [kW]	32.308	31.253	3.3%	30.287	6.3%
Efficiency [%]	94.156	94.285	-0.1%	94.345	-0.2%
Time cost [s]	≈8257	≈631		≈55	

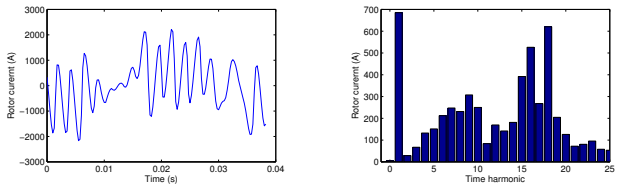

(a) Rotor current (b) Time FFT of rotor current

Fig. 7. Rotor current and its time FFT - loop span 3°

optimization progress. The meshes in the transient model and the static model are almost the same so that we can minimize the influence of the mesh level on the computing time.

D. Limitation of the Model Presented

We save the simulating time at the expense of several limitations of the magneto-static model. The model presented cannot take into account the skin-effect and the proximity-effect because the magneto-static requires the electric conductivity is set as zero. Moreover, the rotor core losses are calculated only with respect to the fundamental frequency f_r because we assume that the main component of the rotor current are with f_r. This is acceptable in the previous case study as mentioned in section(IV-A). However, the situation becomes worse if only one loop locates within one nest and its loop span is quite small. Fig. 7 gives an example for this extreme case. This case is a bad configuration for the BDFIM which should be avoided because it only outputs around 0.3 MW comparing with 3.2 MW of the previous case study with the same size. Actually, for a better BDFIM design, we always pursue a big loop span for a high flux linkage. This makes our static model be not involved in such extreme bad situation. The constrain for the smallest loop span can be used in the optimization to avoid making the static model being inaccurate.

V. CONCLUSION

The adaptive time-step solver is normally used for the transient model in most commercial softwares and the time-step size depends on the convergence and the accuracy. For instance, it needs a small time-step to capture higher time-harmonics in the magnetic fields, as well as in the currents. This paper presents a two-dimensional FE model for the BDFIM based on the magneto-static simulation. Some of the BDFIM performance (e.g. average torque, core losses etc.) can therefore be estimated by several magneto-static simulations.

The number of the magneto-static simulations is determined by the highest frequency considered for the core losses calculation and the simulating period. According to the special space-time relationship of the induced rotor currents in the BDFIM, this paper gives an approximate way to calculate the rotor currents which is not restricted by the time-step. In addition, by considering the space-time transformation again, only one magneto-static simulation is possible to predict the machine performance.

Compared to the results obtained from the transient simulation, it indicates that the presented model can estimate the BDFIM performance at an acceptable accurate level. However, the alternative method can reduce the computing time significantly which makes it possible to be combined with the optimization progress. The model presented has been applied for the optimization of the prototype [13] and the validation of the FE model will be performed on the prototype in the near future. Therefore, the presented FE model based on the magneto-static simulation constitutes a valuable tool in the design of the BDFIM.

REFERENCES

[1] H. Polinder, *Overview of and Trends in Wind Turbine Generator Systems*, Proceedings of the IEEE Power and Energy Society General Meeting, Jul. 2011.

[2] A. R. W. Broadway and L. Burbridge, *Self-cascaded Machine: a Low-Speed Motor or High Frequency Brushless Alternator*, Proceedings, Institution of Electrical Engineers, vol.117, 1970.

[3] R. A. McMahon, X. Wang, E. Abdi-Jalebi, P. J. Tavner, P. C. Roberts, and M. Jagiela, *The BDFM as a Generator in Wind Turbines*, in Power Electronics and Motion Control Conference, 2006. EPE-PEMC 2006. 12th International, Sept. 2006.

[4] H. Polinder, J. A. Ferreira, B. B. Jensen, A. B. Abrahamsen, K. Atallah and R. A. McMahon, *Trends in Wind Turbine Generator Systems*, IEEE Journal of Emerging and Selected Topics in Power Electronics, vol.1, no.3, Sept. 2013.

[5] T. Long, S. Shao, D. Abdi, R. A. McMahon, S. Liu, *Asymmetrical Low-Voltage Ride Through of Brushless Doubly Fed Induction Generator for the Wind Power Generation*, IEEE Trans. on Energy Conversion, vol.28, no.3, pp.502-511, Sept. 2013.

[6] R. A. McMahon, P. C. Roberts, X. Wang and P. J. Tavner, *Performance of BDFM as Generator and Motor*, IEE Proc. Electr. Power Appl., vol.153, no.2, pp.289-299, Mar. 2006.

[7] X. Wang, P. C. Roberts and R. A. McMahon, *Optimization of BDFM Stator Design Using an Equivalent Circuit Model and a Search Method*, The 3rd IET International Conference on Power Electronics, Machines and Drives, 2006.

[8] T. D. Strous, N. H. van der Blij, H. Polinder and J. A. Ferreira, *Brushless Doubly-Fed Induction Machines: Magnetic Field Modelling*, XXI International Conference on Electrical Machines(ICEM'2014), Berlin, Germany, Sept. 2014.

[9] H. Gorginpoer, H. Oraee and R. A. McMahon, *A Novel Modeling Approach for Design Studies of Brushless Doubly Fed Induction Generator Based on Magnetic Equivalent Circuit*, IEEE Trans. on Energy Conversion, vol.28, no.4, Dec. 2013.

[10] A. C. Ferreira and S. Williamson, *Time-stepping Finite-Element Analysis of Brushless Doubly Fed Machine Taking Iron Loss and Saturation into Account*, IEEE Trans. on Industry Applications, vol.35, no.3, 1999.

[11] G. Y. Sizov, D. M. Ionel, and N. A. O. Demerdash, *Modeling and Parametric Design of Permanent-Magnet AC Machines Using Computationally Efficient Finite-Element Analysis*, Industrial Electronics, IEEE Transactions on, vol.59, pp.2403-2413, Jun. 2012.

[12] D. M. Ionel and M. Popescu, *Ultrafast Finite-Element Analysis of Brushless PM Machines Based on Space-Time Transformations*, Industry Applications, IEEE Transactions on, vol.47, pp.744-753, Mar. 2011.

[13] T. D. Strous, Xuezhou Wang, H. Polinder and J. A. Ferreira, *Finite Element Based Multi-Objective Optimization of a Brushless Doubly-Fed Induction Machine*, Electric Machines & Drives Conference (IEMDC), 2015 IEEE International, Coeur d'Alene, USA, May. 2015, to be published.

[14] N. H. van der Blij, T. D. Strous, Xuezhou Wang and H. Polinder, *A Novel Analytical Approach and Finite Element Modelling of a BDFIM*, XXI International Conference on Electrical Machines(ICEM'2014), Berlin, Germany, Sept. 2014.

[15] H. Gorginpoer, H. Oraee and E. Abdi, *Calculation of Core and Stray Load Losses in Brushless Doubly Fed Induction Generators*, IEEE Trans. on Industrial Electronics, vol.61, no.7, Jul. 2014.

VI. BIOGRAPHIES

Xuezhou Wang received the M.Sc. degree in power electronics and electrical drives from Northwestern Polytechnical University, Xi'an, China, in 2013. Currently, he is working towards his Ph.D. degree in the field of electrical machines. His current research interests include numerical modeling and design of electrical machines.

Tim D. Strous received the M.Sc. degree in electrical engineering from Delft University of Technology, Delft, The Netherlands, in 2010. Currently, he is working towards the Ph.D. degree in the field of electrical machines. His current research interests include modeling and design of electrical machines and drives.

Domenico Lahaye received the M.Sc. degree in applied mathematics from the Free University of Brussels, Brussels, Belgium, in 1994, the postgraduate degree in mathematics from the Eindhoven University of Technology, Eindhoven, The Netherlands, in 1996, and the Ph.D. degree in computer science from the Katholic University of Leuven, Leuven, Belgium, in 2001. After having held positions at the Center for Advanced Studies, Research and Development in Sardinia and at the National Research Center for Mathematics and Computer Science in The Netherlands, he joined the Numerical Analysis Research Group, Delft Institute of Applied Mathematics, Delft University of Technology, Delft, The Netherlands, in 2007.

Henk Polinder received the MSc and the PhD degree from Delft University of Technology, Delft, The Netherlands, in 1992 and 1998. Since 1996 he has been an assistant/associate professor in the Electrical Power Processing Group of Delft University of Technology. He worked part-time at Lagerwey in Barneveld in 1998/1999, at Philips Applied Technologies in Eindhoven in 2002 and at ABB Corporate Research in Vasteras in 2008. He was a visiting professor at the University of Newcastle-upon-Tyne in 2002, at Laval University, Quebec in 2004 and at the University of Edinburgh in 2006. He is author or coauthor of over 200 papers. His research interests include design aspects of electrical machines, mainly for renewable energy applications.

Jan A. Ferreira received the B.Sc.Eng., M.Sc..Eng., and Ph.D. degrees in Electrical Engineering from the Rand Afrikaans University, Johannesburg, South Africa in 1981, 1983 and 1988 respectively. In 1981 he was with the Institute of Power Electronics and Electric Drives, Technical University of Aachen, and worked in industry at ESD (Pty) Ltd from 1982-1985. From 1986 until 1997 he was at the Faculty of Engineering, Rand Afrikaans University, where he held the Carl and Emily Fuchs Chair of Power Electronics in later years. Since 1998 he is a professor at the Delft University of Technology in The Netherlands. Dr. Ferreira is a fellow of the IEEE.